



Cite this: DOI: 10.1039/c9nj05404a

A new visible light triggered Arrhenius photobase and its photo-induced reactions†

 Joonyoung F. Joung,[‡] Jeeun Lee,[‡] Joungin Hwang, Kihang Choi* and Sungham Park *

Arrhenius photobases are of potential use for excited state hydroxide ion dissociation (ESHID), photo-induced pOH jump experiments, and base-catalyzed reactions. However, previously studied Arrhenius photobases have to be excited by UV light and undergo ESHID reactions only in protic solvents. These characteristics have become a disadvantage to their application in many fields of research. In this work, we have designed and synthesized a new Arrhenius photobase (NO₂-Acr-OH), the ESHID reaction of which is readily triggered by visible light excitation. In contrast to previously studied Arrhenius photobases, NO₂-Acr-OH undergoes ESHID reactions in protic solvents as well as in polar aprotic solvents. Solvent-dependent photo-induced reactions of NO₂-Acr-OH are comprehensively studied by time-resolved fluorescence spectroscopy. Molecular designs for visible light triggered acridinol-based Arrhenius photobases with a large ΔpK_b value are proposed.

 Received 29th October 2019,
 Accepted 18th December 2019

DOI: 10.1039/c9nj05404a

rsc.li/njc

I. Introduction

A sudden change in the pH of a solution can be made optically by using various photoacids which release protons upon electronic excitation because their pK_a value is significantly decreased in their electronic excited state.^{1–16} As a counterpart of photoacids, quinolines,^{17,18} aminoanthraquinone,¹⁹ 3-styrylpyridine,²⁰ xanthone,²¹ curcumin,²² and Schiff bases^{23,24} have been reported as Brønsted-Lowry photobases which accept protons upon electronic excitation because their pK_a value is increased in their electronic excited state. Based on their interesting photochemical properties, the photoacids and Brønsted-Lowry photobases have been extensively used for a model system to investigate the excited-state proton transfer reaction, proton solvation, ionic effect on the proton transfer reaction, and pH jump induced protein folding.^{1–14,17–24}

As opposed to the Brønsted-Lowry photobases, Arrhenius photobases are capable of releasing hydroxide ions (OH[−]) directly upon electronic excitation. Triphenylmethanol derivatives,^{25–28} 9-phenyl-xanthen-9-ol derivatives,^{29,30} 9-phenyl-acridin-9-ol derivatives,^{31,32} and fluoren-9-ol^{33,34} have been studied as Arrhenius photobases. The excited state hydroxide ion dissociation (ESHID) reactions of several Arrhenius photobases have been studied in water and acetonitrile (ACN) mixtures.³⁰ In addition, Arrhenius photobases have been studied for colorimetric and

fluorometric pH indicators in aqueous and alcohol solutions because their optical properties are sensitive to pH.²⁹ Furthermore, light-driven pOH jump experiments have been carried out by using Arrhenius photobases.²⁵ As such, Arrhenius photobases are of potential use for various fundamental studies and applications. However, for previously reported Arrhenius photobases, their ESHID reactions have been shown to be triggered by UV light excitation and are found to occur only in protic solvents. UV light excitation may hinder the potential use of currently available Arrhenius photobases ($\lambda_{\text{Abs}}^{\text{max}} < \sim 310$ nm) for applications in materials sciences because highly energetic UV photons can cause degradation of materials under study. Furthermore, biological applications of existing Arrhenius photobases may be limited due to their spectral interferences with amino acids such as tryptophan, tyrosine, and phenylalanine which have strong absorption at 260–310 nm.

In this work, we have designed and synthesized a new Arrhenius photobase, the photoreactions of which can be readily triggered by visible light excitation. Photo-induced reactions of the newly designed Arrhenius photobase NO₂-Acr-OH shown in Fig. 1 are studied in various solvents in great detail.

II. Results and discussion

II-A. Designing an Arrhenius photobase with visible light absorption

Acridinol-based photobases (X-Ph-Acr-OH, X = CN, CF₃, H, OCH₃, N(CH₃)₂ and Y = H) shown in Fig. 1 have been studied as Arrhenius photobases, the ESHID reactions of which can

Department of Chemistry and Research Institute for Natural Science, Korea University, Seoul, 02841, Korea. E-mail: kchoi@korea.ac.kr, spark8@korea.ac.kr

† Electronic supplementary information (ESI) available. See DOI: 10.1039/c9nj05404a

‡ These authors contributed equally to this work.

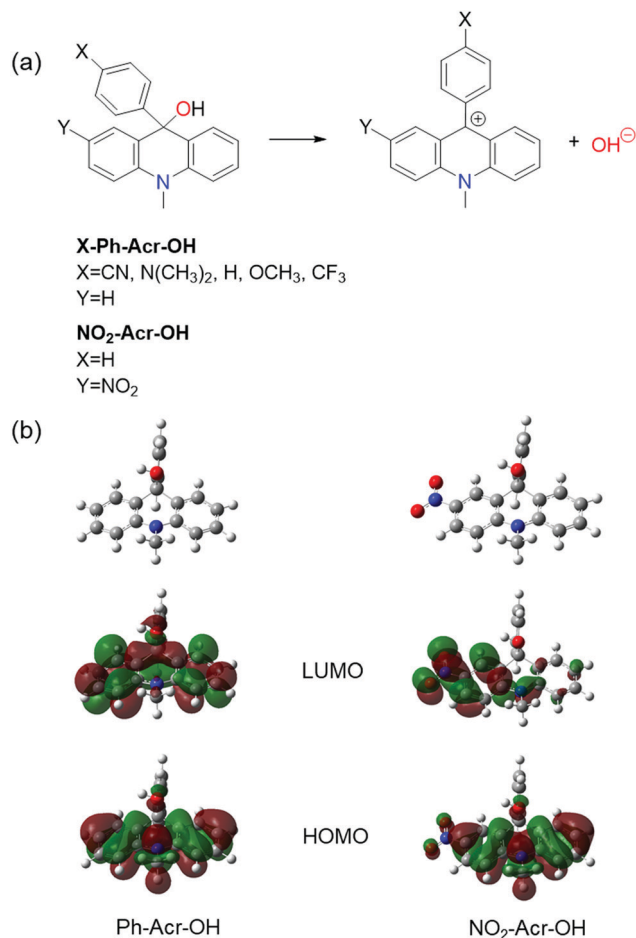


Fig. 1 (a) Molecular structures of acridinol-based photobases and their ESHID reactions. (b) Frontier orbitals of Ph-Acr-OH and $\text{NO}_2\text{-Acr-OH}$. $\text{NO}_2\text{-Acr-OH}$ exhibits more charge transfer (CT) character than Ph-Acr-OH.

occur by absorption of UV light at ~ 310 nm.³² The functional groups ($X = \text{CN}, \text{CF}_3, \text{OCH}_3,$ and $\text{N}(\text{CH}_3)_2$) are introduced at the *para* position (X) of the 9-phenyl group in X-Ph-Acr-OH. DFT calculations indicate that the 9-phenyl group in X-Ph-Acr-OH is perpendicular to the acridine backbone as shown in Fig. 1(b) and it does not influence the conjugation of the acridine backbone significantly. Accordingly, the absorption spectra of acridinol derivatives (X-Ph-Acr-OH) are found to be not much different. However, the absorption and emission spectra of X-Ph-Acr⁺ are significantly influenced by the functional groups at the X position because the 9-phenyl group is placed in the same plane with the acridine backbone in X-Ph-Acr⁺ forming an extended conjugated structure. Based on the relationship between the optical properties and the molecular structures of acridinol-based photobases, we designed a new visible light triggered photobase by introducing a nitro group at the Y position of the acridine backbone shown in Fig. 1 and extending the conjugation of the acridine backbone. This newly designed Arrhenius photobase ($\text{NO}_2\text{-Acr-OH}$) in various solvents is found to be readily excited by ~ 400 nm light and undergoes ESHID reaction and intersystem crossing, which will be discussed below in great detail.

II-B. Photophysical properties of $\text{NO}_2\text{-Acr-OH}$ in water

Fig. 2(a) displays the UV-visible absorption spectra of $\text{NO}_2\text{-Acr-OH}$ and $\text{NO}_2\text{-Acr}^+$ in water, which are significantly red-shifted due to the nitro group which increases the conjugation length of the acridine backbone. In addition, the nitro group is found to destabilize $\text{NO}_2\text{-Acr}^+$ because of its electron withdrawing ability which leads to a significant increase in the $\text{p}K_b$ value of $\text{NO}_2\text{-Acr-OH}$. The $\text{p}K_b$ value of $\text{NO}_2\text{-Acr-OH}$ in water was theoretically estimated to be 7.69 by using eqn (S3) (ESI[†]) and DFT calculations, and was experimentally determined to be 7.63 at 25 °C as described in the ESI[†] (Fig. S1–S5).^{35–41} Obviously, the $\text{p}K_b$ value of $\text{NO}_2\text{-Acr-OH}$ is larger than that of X-Ph-Acr-OH shown in Fig. 1(a) which is in the range of 2.3 to 3.3.

Fig. 2(b) shows the photoluminescence (PL) spectra of $\text{NO}_2\text{-Acr-OH}$ and $\text{NO}_2\text{-Acr}^+$ in water. The PL quantum yields of $\text{NO}_2\text{-Acr-OH}$ and $\text{NO}_2\text{-Acr}^+$ in water are determined to be $\Phi_{\text{PLQY}} = 0.003$ and 0.010, respectively (Fig. S6, ESI[†]).⁴² The PL of $\text{NO}_2\text{-Acr-OH}$ in water is negligibly weak. Two peaks are observed in the PL spectrum of $\text{NO}_2\text{-Acr-OH}$ in water (see the inset of Fig. 2(b)). The PL peaks at ~ 450 nm and ~ 550 nm are found to result from photo-generated $\text{NO}_2\text{-Acr}^+$ and $\text{NO}_2\text{-Acr-OH}$, respectively, as will be discussed in the next section. Because of

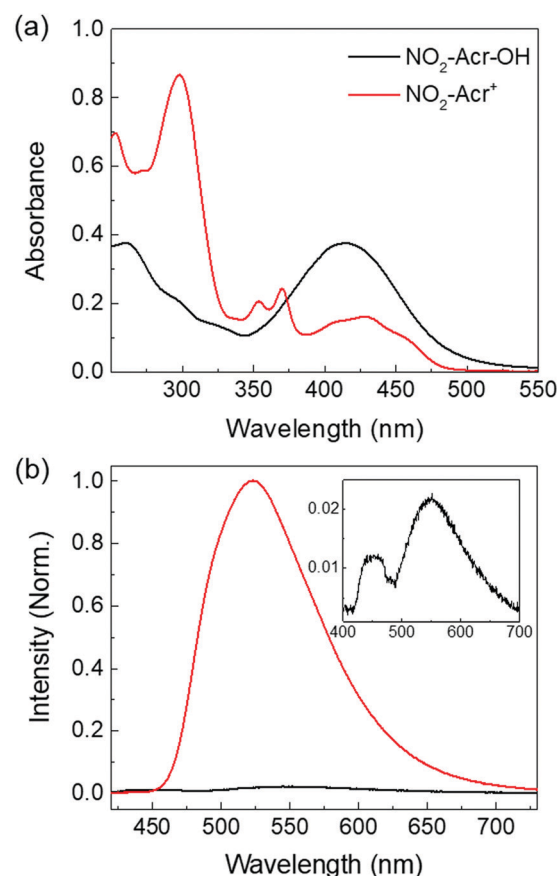


Fig. 2 (a) UV-visible absorption spectra of $\text{NO}_2\text{-Acr-OH}$ and $\text{NO}_2\text{-Acr}^+$ in water (38 μM). (b) PL spectra of $\text{NO}_2\text{-Acr-OH}$ (black) and $\text{NO}_2\text{-Acr}^+$ (red) in water ($\lambda_{\text{ex}} = 375$ nm) and their relative intensities are compared. The inset shows the emission spectrum of $\text{NO}_2\text{-Acr-OH}$ on a different intensity scale.

such negligible fluorescence intensity, the photo-induced reaction of $\text{NO}_2\text{-Acr-OH}$ in water is unable to be studied by time-resolved fluorescence experiments.

II-C. Photo-induced reaction of $\text{NO}_2\text{-Acr-OH}$ in organic solvents

The UV-visible absorption and emission spectra of $\text{NO}_2\text{-Acr-OH}$ are measured in various solvents (dimethyl sulfoxide (DMSO), acetonitrile (ACN), methanol, ethanol, tetrahydrofuran (THF), and toluene) as shown in Fig. 3. The absorption peaks of $\text{NO}_2\text{-Acr-OH}$ are near 400 nm and are gradually red-shifted as the solvent polarity is increased (solvatochromic shift). The absorption spectra of $\text{NO}_2\text{-Acr}^+$ in organic solvents, which is prepared by the reaction of $\text{NO}_2\text{-Acr-OH}$ with sulfuric acid ($\text{NO}_2\text{-Acr-OH} + \text{H}^+ \rightarrow \text{NO}_2\text{-Acr}^+ + \text{H}_2\text{O}$), are displayed in Fig. 3(b). The ΔpK_b ($=pK_b - pK_b^*$) values of $\text{NO}_2\text{-Acr-OH}$ are estimated to be 2.9, 4.5, 4.4, and 4.7 in DMSO, ACN, methanol, and ethanol, respectively, by using the Förster cycle method.¹⁴ The emission spectra of $\text{NO}_2\text{-Acr-OH}$ (Fig. 3(c)) are solvent-dependent, which results from different photo-induced processes occurring in various solvents as will be presented in the next section.

To study the photo-induced reaction of $\text{NO}_2\text{-Acr-OH}$ in different solvents, we carried out time-resolved fluorescence (TRF) experiments by using the time-correlated single photon counting (TCSPC) method. Fig. 4 shows the TRF signals measured with $\text{NO}_2\text{-Acr-OH}$ in different solvents following excitation by 375 nm pulses. Note that the TRF signals measured at ~ 400 nm are found to be readily quenched by molecular oxygen (O_2) as shown in Fig. S7 (ESI[†]) and are attributed to the phosphorescence of $\text{NO}_2\text{-Acr-OH}$. This feature has been commonly observed with previously studied Arrhenius photobases.^{30–34} However, the TRF signals measured at ~ 600 nm, which are not quenched by O_2 as shown in Fig. S8 (ESI[†]), result from the fluorescence of $\text{NO}_2\text{-Acr-OH}$. Accordingly, to analyze the TRF signals of $\text{NO}_2\text{-Acr-OH}$, the ESHID reaction and intersystem crossing (ISC) process are included in the kinetic model presented in Fig. 4(a).

In the kinetic model shown in Fig. 4(a), k_{ROH} , k_{R^+} , and k_{triplet} are the rate constants for the radiative decay of $\text{NO}_2\text{-Acr-OH}^*$, $\text{NO}_2\text{-Acr}^{+*}$, and $^3[\text{NO}_2\text{-Acr-OH}^*]$, respectively. The rate constants for ESHID and reverse ESHID reactions are k_{OH} and k_{rev} , respectively, and k_{ISC} is the ISC rate constant. By using the global fitting analysis based on the kinetic model,^{9,43–45} the TRF signals of $\text{NO}_2\text{-Acr-OH}$ were fully analyzed and all the rate constants were extracted as summarized in Table 1. The individual contributions of $\text{NO}_2\text{-Acr-OH}^*$, $\text{NO}_2\text{-Acr}^{+*}$, and $^3[\text{NO}_2\text{-Acr-OH}^*]$ to each TRF signal exhibit distinct spectral and temporal features as shown in Fig. 4.

The global fitting analysis of TRF signals reveals a few interesting and important features. First, the ESHID reaction of $\text{NO}_2\text{-Acr-OH}$ does not occur in weakly polar solvents (THF and toluene). In this case, the produced $\text{NO}_2\text{-Acr}^+$ may not be stabilized in THF ($\epsilon = 7.52$) and toluene ($\epsilon = 2.38$) with small dielectric constants (ϵ).³⁷ Second, the ESHID reaction and the ISC process occur competitively in polar solvents but the ESHID reaction is relatively faster than the ISC process ($k_{\text{OH}} > k_{\text{ISC}}$). Third, the ESHID reaction of $\text{NO}_2\text{-Acr-OH}$ is much faster in polar protic solvents (methanol and ethanol) than in polar

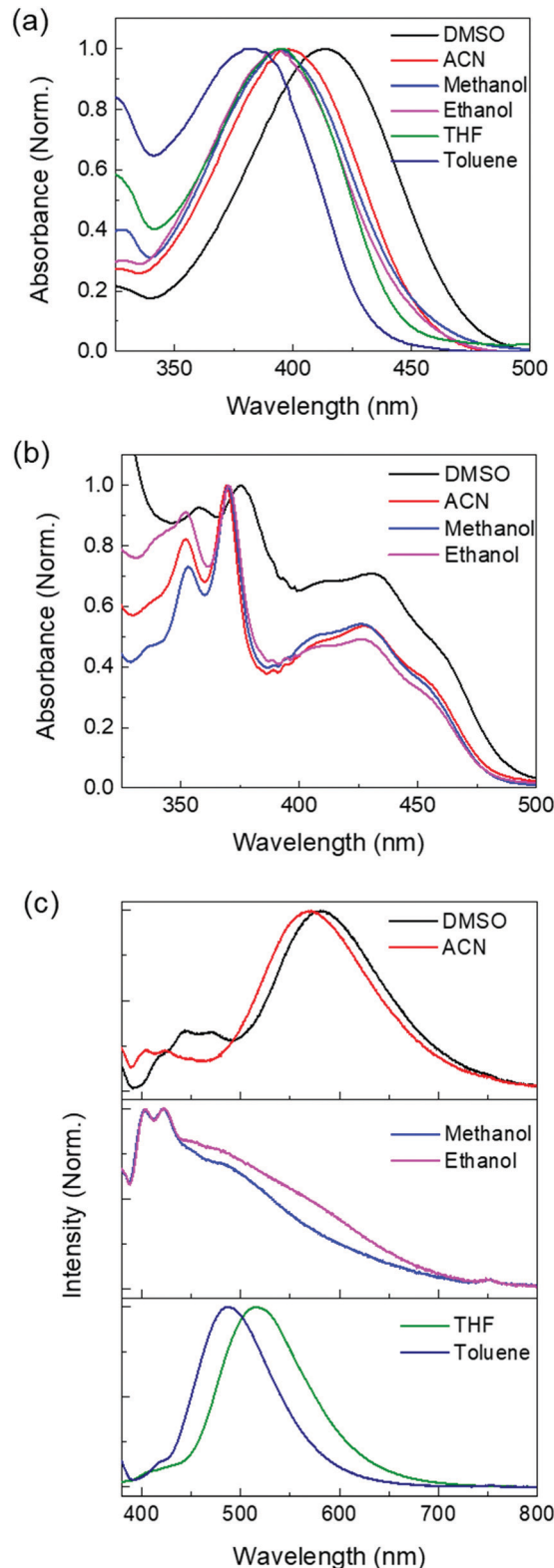


Fig. 3 (a) UV-visible absorption spectra of $\text{NO}_2\text{-Acr-OH}$ in various solvents. (b) UV-visible absorption spectra of $\text{NO}_2\text{-Acr}^+$ in various solvents. (c) PL spectra of $\text{NO}_2\text{-Acr-OH}$ in various solvents ($\lambda_{\text{ex}} = 375$ nm).

aprotic solvents (ACN and DMSO). This implies that the hydroxide ion dissociation reaction of $\text{NO}_2\text{-Acr-OH}$ should occur *via*

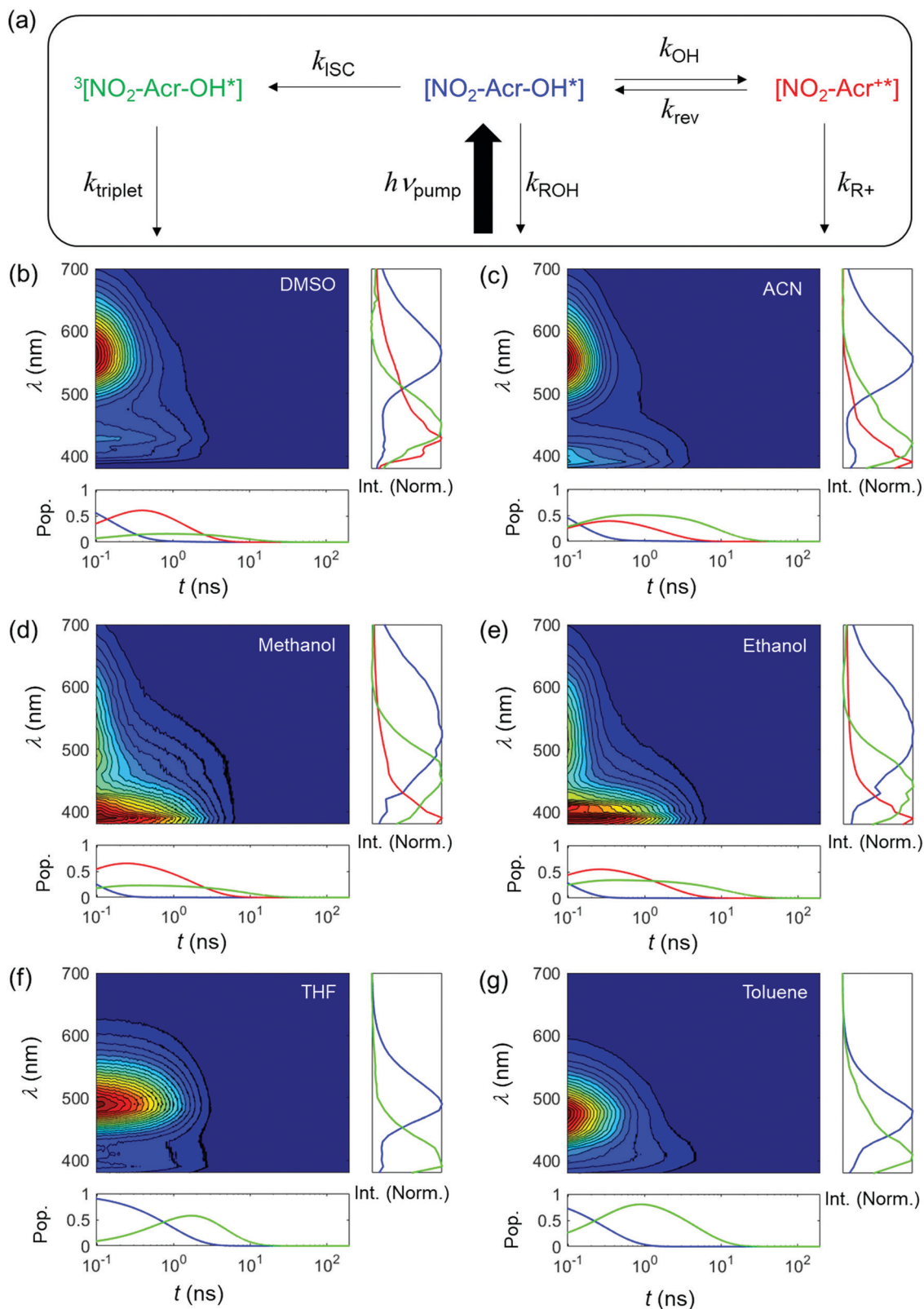


Fig. 4 (a) Kinetic model for analyzing the TRF signals of NO₂-Acr-OH in various solvents. TRF signals measured with NO₂-Acr-OH in (b) DMSO, (c) ACN, (d) methanol, (e) ethanol, (f) THF, and (g) toluene ($\lambda_{ex} = 375$ nm). The spectral components and time-dependent population decay of NO₂-Acr-OH* (blue), NO₂-Acr⁺⁺ (red), and ³[NO₂-Acr-OH*] (green), which are extracted from the global fitting analysis, are presented in the right and bottom panels, respectively.

Table 1 Rate constants extracted from the global fitting analysis

	k_{OH} (ns ⁻¹)	k_{rev} (ns ⁻¹)	k_{ISC} (ns ⁻¹)	k_{ROH} (ns ⁻¹)	k_{R^+} (ns ⁻¹)	k_{triplet}^a (ns ⁻¹)	Φ_{OH}^b
DMSO	5.03	0.18	0.93	0.099	0.651	0.015	0.83
ACN	4.50	0.27	3.71	0.103	0.428	0.013	0.54
Methanol	10.63	0.05	3.40	0.247	0.542	0.012	0.74
Ethanol	8.19	0.05	4.53	0.167	0.534	0.016	0.64
THF	—	—	1.00	0.078	—	0.009	—
Toluene	—	—	3.20	0.091	—	0.012	—

^a k_{triplet} is determined by TRF experiments with NO₂-Acr-OH in degassed solvents. ^b $\Phi_{\text{OH}} = k_{\text{OH}}/(k_{\text{OH}} + k_{\text{ISC}} + k_{\text{ROH}})$.

Table 2 The pK_{b} and pK_{b}^* values of NO₂-Acr-OH in various organic solvents

	DMSO	ACN	Methanol	Ethanol
pK_{b}	1.5	3.3	2.1	2.5
pK_{b}^*	-1.4	-1.2	-2.3	-2.2

acid-catalytic processes. Lastly, the pK_{b}^* values of NO₂-Acr-OH in various solvents were estimated by the rate constants, *e.g.*, $pK_{\text{b}}^* = -\log_{10}(k_{\text{OH}}/k_{\text{rev}})$, by assuming that the ESHID equilibrium was rapidly achieved in the electronic excited state. Subsequently, the pK_{b} values were determined by using the Förster cycle method and the pK_{b}^* values (Table 2). The OH⁻ dissociation rate (k_{OH}) (Table 1) is shown to become larger as the pK_{b}^* value gets smaller, which has been explained by the free-energy-reactivity relationship in the literature.^{30,32} The quantum yield of OH⁻ production indicates that the OH⁻ dissociation in excited state is more favored than the ISC process in polar solvents.

Before this section is closed, it should be noted that acridinol-based photobases (X-Ph-Acr-OH, X = CN, CF₃, H, CH₃O, and (CH₃)₂N) in various solvents have been studied by Glusac and co-workers.^{31,32} They have found that X-Ph-Acr-OH in S₁ state undergoes ESHID reaction and ISC process in alcohol but not in polar aprotic solvents (*e.g.*, ACN). In addition, they have claimed that the ground state X-Ph-Acr⁺ is directly formed as a result of the ESHID reaction of X-Ph-Acr-OH. In contrast, our new NO₂-Acr-OH is found to undergo ESHID reaction in both polar aprotic and protic solvents producing fluorescent NO₂-Acr⁺. The nitro group introduced to the acridine backbone makes significant changes in the chemical and photo-physical properties of acridinol-based Arrhenius photobases in terms of the absorption spectrum, pK_{b} value, and solvent-dependent ESHID reaction.

III. Concluding remarks

A new Arrhenius photobase, NO₂-Acr-OH, which was readily excited by visible light, was designed and synthesized and its photo-induced reactions were comprehensively studied in various solvents by using steady-state fluorescence and TRF experiments combined with DFT calculations. Unlike previously studied Arrhenius photobases, the ESHID reaction of NO₂-Acr-OH was found to occur not only in protic solvents but also in polar aprotic solvents. The ESHID reaction was dependent on solvent polarity. The ESHID reaction was relatively fast in highly polar solvents and protic solvents but did not proceed in weakly

polar solvents. In addition, NO₂-Acr-OH was found to undergo ISC process in various solvents but the ISC process of NO₂-Acr-OH was not significantly solvent-dependent. Note that NO₂-Acr-OH in water exhibits weak fluorescence ($\Phi_{\text{PLQY}} = 0.003$) and undergoes ESHID reactions producing NO₂-Acr⁺ whose fluorescence is negligibly weak as well. Therefore, NO₂-Acr-OH is nearly a non-fluorescent Arrhenius photobase in aqueous solutions and can be used in pOH jump experiments minimizing its fluorescence interference with molecular systems under study.

Visible light triggered photobases with large ΔpK_{b} values are ideal for studying ESHID reactions in various molecular systems. NO₂-Acr-OH absorbs visible light but exhibits a relatively small ΔpK_{b} value. In the case of Ph-Acr-OH, functionalizing the *para* position of the 9-phenyl group is shown to increase the ΔpK_{b} value while functionalizing the acridine backbone induces a redshift in the absorption of photobases. Accordingly, we will be able to develop various visible light triggered Arrhenius photobases with large ΔpK_{b} values by introducing different functional groups at the *para* position of the 9-phenyl group and in the acridine backbone.

Conflicts of interest

There are no conflicts of interest to declare.

Acknowledgements

This study was supported by grants from the National Research Foundation of Korea (NRF) funded by the Korean government (MSIP) (No. 2019R1H1A2079968 and 2019R1A6A1A11044070 for S. P. and No. 20100020209 for K. C.).

References

- 1 E. Pines and D. Huppert, *J. Phys. Chem.*, 1983, **87**, 4471–4478.
- 2 S. Abbruzzetti, E. Crema, L. Masino, A. Vecchi, C. Viappiani, J. R. Small, L. J. Libertini and E. W. Small, *Biophys. J.*, 2000, **78**, 405–415.
- 3 M. Rini, B. Z. Magnes, E. Pines and E. T. Nibbering, *Science*, 2003, **301**, 349–352.
- 4 M. Rini, D. Pines, B. Z. Magnes, E. Pines and E. T. Nibbering, *J. Chem. Phys.*, 2004, **121**, 9593–9610.
- 5 N. Agmon, *J. Phys. Chem. A*, 2005, **109**, 13–35.
- 6 D. B. Spry and M. D. Fayer, *J. Chem. Phys.*, 2008, **128**, 084508.

- 7 Y.-S. Lee, O.-H. Kwon, H. J. Park, J. Franz and D.-J. Jang, *J. Photochem. Photobiol., A*, 2008, **194**, 105–109.
- 8 M. J. Cox, B. J. Siwick and H. J. Bakker, *ChemPhysChem*, 2009, **10**, 236–244.
- 9 J. F. Joung, S. Kim and S. Park, *J. Phys. Chem. B*, 2015, **119**, 15509–15515.
- 10 R. Simkovitch, S. Shomer, R. Gepshtein and D. Huppert, *J. Phys. Chem. B*, 2015, **119**, 2253–2262.
- 11 S. P. Laptanok, J. Conyard, P. C. Page, Y. Chan, M. You, S. R. Jaffrey and S. R. Meech, *Chem. Sci.*, 2016, **7**, 5747–5752.
- 12 W. Liu, Y. Wang, L. Tang, B. G. Oscar, L. Zhu and C. Fang, *Chem. Sci.*, 2016, **7**, 5484–5494.
- 13 J. F. Joung, S. Kim and S. Park, *Phys. Chem. Chem. Phys.*, 2017, **19**, 25509–25517.
- 14 J. F. Joung, S. Kim and S. Park, *J. Phys. Chem. B*, 2018, **122**, 5087–5093.
- 15 A. A. Awasthi and P. K. Singh, *ChemPhysChem*, 2018, **19**, 198–207.
- 16 O. Gajst, L. Pinto da Silva, J. C. G. Esteves da Silva and D. Huppert, *J. Phys. Chem. A*, 2019, **123**, 48–58.
- 17 N. Munitz, Y. Avital, D. Pines, E. T. J. Nibbering and E. Pines, *Isr. J. Chem.*, 2009, **49**, 261–272.
- 18 E. W. Driscoll, J. R. Hunt and J. M. Dawlaty, *J. Phys. Chem. A*, 2017, **121**, 7099–7107.
- 19 T. Yatsushashi and H. Inoue, *J. Phys. Chem. A*, 1997, **101**, 8166–8173.
- 20 G. Favaro, U. Mazzucato and F. Masetti, *J. Phys. Chem.*, 1973, **77**, 601–604.
- 21 B. S. Vogt and S. G. Schulman, *Chem. Phys. Lett.*, 1983, **97**, 450–453.
- 22 K. Akulov, R. Simkovitch, Y. Erez, R. Gepshtein, T. Schwartz and D. Huppert, *J. Phys. Chem. A*, 2014, **118**, 2470–2479.
- 23 A. Jimenez-Sanchez and R. Santillan, *Analyst*, 2016, **141**, 4108–4120.
- 24 W. Sheng, M. Nairat, P. D. Pawlaczyk, E. Mroczka, B. Farris, E. Pines, J. H. Geiger, B. Borhan and M. Dantus, *Angew. Chem., Int. Ed.*, 2018, **57**, 14742–14746.
- 25 M. Irie, *J. Am. Chem. Soc.*, 1983, **105**, 2078–2079.
- 26 S. Abbruzzetti, M. Carcelli, P. Pelagatti, D. Rogolino and C. Viappiani, *Chem. Phys. Lett.*, 2001, **344**, 387–394.
- 27 L. Zhou, H. Yang and P. Wang, *J. Org. Chem.*, 2011, **76**, 5873–5881.
- 28 X. Ding and P. Wang, *J. Org. Chem.*, 2018, **83**, 10736–10742.
- 29 E. E. Nekongo, P. Bagchi, C. J. Fahrni and V. V. Popik, *Org. Biomol. Chem.*, 2012, **10**, 9214–9218.
- 30 Y. Xie, H. L. Luk, X. Yang and K. D. Glusac, *J. Phys. Chem. B*, 2015, **119**, 2498–2506.
- 31 D. Zhou, R. Khatmullin, J. Walpita, N. A. Miller, H. L. Luk, S. Vyas, C. M. Hadad and K. D. Glusac, *J. Am. Chem. Soc.*, 2012, **134**, 11301–11303.
- 32 Y. Xie, S. Ilic, S. Skaro, V. Maslak and K. D. Glusac, *J. Phys. Chem. A*, 2017, **121**, 448–457.
- 33 E. Gaillard, M. A. Fox and P. Wan, *J. Am. Chem. Soc.*, 1989, **111**, 2180–2186.
- 34 R. A. McClelland, N. Mathivanan and S. Steenken, *J. Am. Chem. Soc.*, 1990, **112**, 4857–4861.
- 35 J. Kielland, *J. Am. Chem. Soc.*, 1937, **59**, 1675–1678.
- 36 S. Park, C. Kim, M. H. Kim, I.-J. Lee and K. Kim, *J. Chem. Soc., Faraday Trans.*, 1998, **94**, 1421–1425.
- 37 D. R. Lide, *CRC Handbook of chemistry and physics*, CRC Press, Boca Raton, Florida, 83rd edn, 2002.
- 38 A. V. Marenich, C. J. Cramer and D. G. Truhlar, *J. Phys. Chem. B*, 2009, **113**, 6378–6396.
- 39 T. Matsui, A. Oshiyama and Y. Shigeta, *Chem. Phys. Lett.*, 2011, **502**, 248–252.
- 40 T. Matsui, T. Baba, K. Kamiya and Y. Shigeta, *Phys. Chem. Chem. Phys.*, 2012, **14**, 4181–4187.
- 41 T. Matsui, Y. Shigeta and K. Morihashi, *J. Chem. Theory Comput.*, 2017, **13**, 4791–4803.
- 42 A. M. Brouwer, *Pure Appl. Chem.*, 2011, **83**, 2213–2228.
- 43 J. F. Joung, J. Baek, Y. Kim, S. Lee, M. H. Kim, J. Yoon and S. Park, *Phys. Chem. Chem. Phys.*, 2016, **18**, 23096–23104.
- 44 J. Baek, J. F. Joung, S. Lee, H. Rhee, M. H. Kim, S. Park and J. Yoon, *J. Phys. Chem. Lett.*, 2016, **7**, 259–265.
- 45 K. Y. Oang, C. Yang, S. Muniyappan, J. Kim and H. Ihee, *Struct. Dyn.*, 2017, **4**, 044013.